AIAA 90-0224

Large-Amplitude High-Rate Roll Experiments on a Delta and Double Delta Wing

E.S. Hanff and S.B. Jenkins
National Aeronautical Establishment
Ottawa, Canada

28th Aerospace Sciences Meeting
8-11 January 1990 / Reno, NV

For permission to copy or republish, contact the National Research Council of Canada

AIAA-90-0224

Large-Amplitude High-Rate Roll Experiments on a Delta and Double Delta Wing*

E.S. Hanff† and S.B. Jenkins‡
National Aeronautical Establishment
Ottawa, Canada

Abstract

A comprehensive wind-tunnel test program on both a 65º delta an 80º/65º double delta wing model has been recently completed. The program included static and dynamic force tests. A brief description of the various experiments is presented, as well as results that demonstrate the value of the previously proposed "hypersurface" representation of aerodynamic loads in the non-linear and unsteady regimes.

1 Symbols

b	Span	
k	Reduced frequency	$\frac{b}{2V}\omega$
S	Model planform area	
V	Free stream velocity	
ϕ	Roll angle	
$\dot{\phi}$	Reduced roll rate	$\frac{b}{2V}\frac{\partial\phi}{\partial t}$
ϕ_0	Mean roll angle	
$\Delta\phi$	Rolling oscillation amplitude	
?	Circular frequency (rad/s)	

* Work conducted under Joint Research Program of U.S. Airforce Office for Scientific Research and Wright Research and Development Center Flight Dynamics Lab., National Aeronautical Establishment and Canadian Dept. of National Defense.

† Senior Research Officer, Member AIAA
‡ Technical Officer

Copyright © 1990 by the National Research Council of Canada. Published by the American Institute of Aeronautics and Astronautics, Inc. with permission.

2 Introduction

The evolution of high-performance aircraft requires ever-increasing maneuverability and agility capabilities. Current supermaneuverability concepts include situations, such as flight at high angle of attack and motions involving large amplitudes and high angular rates, where severely separated and unsteady flow conditions prevail. Under these conditions, airloads may be highly non-linear in terms of the pertinent motion variables, casting considerable doubt on the effectiveness of the linear mathematical model implicit in the stability derivatives formulation [1,2,3,4].

A different approach to represent aerodynamic reactions, that does not rely on assumptions of linearity, and can thus be used for simulations in the non-linear flight regime, has been proposed [5]. The method is based on the utilization of instantaneous values of the pertinent aerodynamic reactions as forcing functions in the equations of motion, an approach that implies that values of the reactions are known as a function of the motion variables. Special wind-tunnel testing techniques are required to provide the necessary information. One such technique, that permits an efficient measurement of instantaneous values of aerodynamic reactions in terms of the corresponding instantaneous values of the pertinent motion variables, has been developed by the present author [6]. The

measured reactions are stores as a function of the motion variables in look-up tables that can then be used directly in simulations. In a topological sense, the look-up tables that describe the reactions as functions of n motion variables, correspond to reaction hypersurfaces in n+1 dimensions.

A test program designed to verify the effectiveness of the wind-tunnel testing technique as a means to obtain the necessary data, and to establish the value of the hypersurface formulation for flight mechanics applications, has been recently completed at the NAE 6ft x 9ft low speed wind tunnel. It bears mention that the measurement technique and load representation are not only useful as tools to improve flight mechanics predictions, but also as means to increase the understanding of flows in the non-linear regime.

3 Experimental program

A delta wing model was tested in a rather comprehensive program that comprised four main elements, namely: static force measurements, dynamic force measurements in the presence of a large-amplitude high-rate motion, high speed laser sheet flow visualization and free-to-move tests. Because of its relevance to wing rock problems as well as its relatively simple mechanical implementation, a single degree of freedom motion in roll was selected for the program.

The force measurements provided the data base required to conduct single degree-of freedom (roll) simulations that could then be validated through a comparison with the actual motions occurring in the free-to-roll tests. High-speed flow visualization tests were included to provide a better insight of non-linear and unsteady aerodynamics generally and, more specifically, of the mechanisms underlying the measured loads.

4 Roll oscillation rig

A large-amplitude high-rate oscillatory roll rig was used to conduct the experiments (Fig. 1). The motion of the model is imparted by a hydraulic rotary actuator mounted at the aft end of the sting and connected to the rear of a vive-component balance via a carbon composite driveshaft. In order to obtain the desired high amplitudes and frequencies, the hydraulic actuator is driven by a 50 HP power pack and is capable of developing a torque of 3000 in-lb. The balance, specifically designed for this application, must be very strong and stiff and thus, like most balances used in dynamic testing, does not include an axial force capability. Design and construction details of the rig. Hydraulic system and balance can be found elsewhere[7]. The instrumentation and data handling systems have also been described[6,8].

5 Model

The model, a 65º sweep delta wing with interchangeable noses (Fig. 2) is designed to withstand a normal force of 2000 lb while having a very low rolling moment of inertia in order to minimize inertial loads as much as possible. Thus, the wings are made of a multi-layer carbon composite skin with a foam core, whereas the body is entirely carbon composite. A rather elaborate arrangement is used at the wing roots to avoid structural problems due to high local stresses. A steel insert suitably bonded within the body is used to mount the model on the balance. The requirement for

zero backlash in the presence of high alternating aerodynamic and inertial loads arising from roll angular accelerations of up to 11,000 rad/s^2 dictated the use of a polygon taper as the joint between balance and model. The interchangeable noses are made of aluminum alloy and are fastened to a steel tongue imbedded in the forward end of the composite part of the model. The total model weight is 8.3 lb (4.5 lb concentrated in the steel insert) and its rolling moment of inertia is approximately 0.15 lb in s^2.

6 Force tests

Force tests were undertaken to provide adequately populated data bases for the instantaneous aerodynamic reactions as functions of the instantaneous values ofϕ, $\dot{\phi}$ and $\ddot{\phi}$. To this end, both static and dynamic force tests were conducted at a speed of 300 ft/s (Re=1,250.000 per ft) and an angle of attack of up to 40º. In the dynamic tests the model was oscillated sinusoidally in roll with an amplitude 5, 12, 19, 26, 33 and 40 degrees at a frequency reduced frequency and angular rate of 0.2 and 0.15 respectively. In order to independently control ϕ and $\ddot{\phi}$, the oscillations were centered about mean roll angles of 0, 14, 28 and 42 degrees.

Better motion waveforms were obtained by using two different servovalves for tests involving high and low hydraulic flow conditions. Likewise, keeping in mind that these conditions also correspond to high and low dynamic loading, two balances having different strength and sensitivity characteristics, were used to maximize the signals without jeopardizing the balance mechanical integrity.

In as much as each run entailed the acquisition of data for 20-40 seconds, most of the noise was eliminated from the signals by the ensemble average process[6], resulting in very good repeatability. Fig. 3 shows repeat runs conducted with the two balances in combination with the corresponding servovalves. Much of the discrepancy can be accounted for by the slight difference in the motion as indicated by the trajectories on the phase plane.

Tare measurements were done in air due to the impossibility of evacuation the wind tunnel. Moreover, no support or wall interference corrections were attempted. A similar test program to be conducted shortly at another wind tunnel is expected to shed some light on the possible impact of interference effects.

7 Free-to-roll-tests

The free-to-roll tests were included in the program in order to validate the aerodynamic load representation and wind-tunnel technique. This was accomplished by comparing the single DOF motion prediction based on force data with the actual motion obtained under free-to roll conditions. Free-to-roll tests were conducted by modifying the aft end of the rig to include a clutch between the rotary actuator and driveshaft. The model could thus be rotated to any desired initial roll angle, from where it was released by disengaging the clutch. No provision was made to impart an initial angular rate. In order to minimize friction, all bearing seals were removed and light oil used for lubrication. In spite of these precautions, some friction still remained that needs to be accounted for in the simulations.

8 Flow visualization

In order to gain a better understanding of the underlying flow phenomena, the test program included a substantial flow visualization component. Emphasis was placed on the observation of the vortical flow on the lee side of the model. The flow was seeded with a single kerosene vapor dispensing probe located approximately 5 ft upstream of the model nose, which resulted in the smoke plume having a diameter of approximately 3 in. at the impingement location. The exact probe location was selected to maximize the visibility of the wing leading edge vortices.

A conventional light sheet arrangement was used for the flow visualization (Fig. 4). A 15W argon ion laser beam was expanded by a cylindrical lens and then reflected onto the model by a high reflectivity mirror. Illumination of the flow at different model stations was accomplished by mounting the optical components on a traversing mechanism. The large windows in the test section of the wind-tunnel allowed a virtually ideal geometry, in which the light sheet is perpendicular to the model axis and the camera is located exactly in front of the model. Recording was concurrently done with two cameras: a Super VHS studio quality video camera with good sensitivity and resolution but capable of only 30 frames per second, although the shutter aperture time was 1 ms; and a high speed video camera capable of 1000 frames/s. The latter however, exhibited a surprisingly low sensitivity which dictated the use of a wind speed of no more than 210 ft/s (Re=900,000/ft) at a maximum of 250 frame/s. Under these conditions there was a reasonable temporal resolution in the presence of the desired model oscillation amplitudes of up to 40º at 4 and 7 Hz. The roll oscillation was centered about the same mean roll angles as in the force tests. The flow visualization data has only begun to be analyzed at the time of this writing. An example of a single video frame for the model with the 65º nose at an angle of attack of 30º is shown in Fig. 5. The model oscillation is about ϕ_0=14º with an amplitude of 40º and a reduced frequency of 0.11. The view corresponds to a model station at about 80% chord with the right wing moving downwards. Preliminary analysis of the videos has already revealed that very significant dynamic effects, similar to those observed by Arena and Nelson [9] for an 80º sweep delta wing, are present in the bursting point locations of the leading edge vortices.

9 Experimental results

A large body of data was obtained in the test program, much of it not having been fully analyzed to date. Here the results for one specific case will be described, namely, those obtained for the model with the 65º nose at an angle of attack of 30º. Although the load data were obtained as functions of ϕ, $\dot{\phi}$ and $\ddot{\phi}$, the dependence on $\ddot{\phi}$ was not required in the case at hand. This should not be construed as a general conclusion, as it is quite possible that higher time derivatives are necessary in other situations.

The reaction surfaces corresponding to the rolling moment coefficient in terms of ϕ and $\dot{\phi}$ are shown in Fig. 6(1) to (d) for different values of mean roll angle. The surfaces were obtained on the basis of the fundamental frequency component as well as 5 harmonics of the rolling moment. The trajectories on the ϕ-$\dot{\phi}$ phase planes correspond to oscillations with $\Delta\phi$=5, 12, 19, 26, 33 and 40º at k=0.14 and are not

exactly elliptical due to slight distortions of the motion. Note that the surfaces have been offset by C_1=0.1 in order to facilitate viewing and that they use the same axes and perspective.

It has been shown[5] that in this representation the static and dynamic stability derivatives are related to the orientation of the surface relative to the axes at the point of interest, specifically, they are equal to the direction numbers (with respect to ϕ and $\dot{\phi}$ respectively) of the normal to the surface at that point. Moreover, an attractor (trim condition) is present wherever the ϕ axis penetrates the reaction surface at a location exhibiting static and dynamic stability.

Fig. 7 shows the intersections of the reaction surfaces with planes at different values of ϕ. The figures reveal that the surface for ϕ_0=0 is quite distinct from the others which, in fact, tend to coalesce into one, except for the region of ϕ >10º and positive $\dot{\phi}$, where the surface corresponding to ϕ_0=14º is somewhat displaced toward the one for 0º. $C_1\dot{\phi}$ is represented in Fig. 7 by the slopes of the curves, indicating that the damping associated with the ϕ_0=0 surface is generally considerably higher than those for the others.

There seems to be a *prima facie* case for postulating that there are three flow regimes depending on the mean roll angle of the oscillation, where the third regime is represented by the reaction surfaces for negative mean roll angles. As expected, the latter were found to be symmetrical to the corresponding ones for positive ϕ_0. An illustration of this symmetry can be seen in Fig. 8 where the trajectories of the load point for two runs with the same test conditions but with ϕ_0=14º and -14º are shown. The sign of the coordinates for the latter were reversed in order to superimpose the two curves. The intersection of the reaction surfaces with the plane $\dot{\phi}$=0 (Fig. 9) shows that those corresponding to $\phi_0 \neq 0$ coalesce (at least for $\dot{\phi}$=0) up to the largest roll angles encountered. The static rolling moment coefficient (solid triangles) at non-zero roll angle can be seen to coincide with the surface corresponding to finite ϕ_0, indicating a negligible rolling acceleration effect. Likewise, the static coefficient at ϕ=0 coincides with the surface for that mean roll angle. The figure also shows that the stiffness associated with the ϕ_0=0 reaction surface is higher than those for $\phi_0 \neq 0$.

Fig. 9 indicates that there is a statically stable point at ϕ=21º which Fig. 7 (c) shows to be also dynamically stable. Keeping in mind the definition of attractors and the symmetry of the reaction surfaces, it follows that there are attractors at ϕ=±21º. It is interesting to note, however, that on the basis of the static data available, the crossing at the origin is unstable, precluding the possibility of a trim condition at ϕ=0. Significantly, however, the ϕ_0=0 reaction surface does have an attractor at the origin (Figs. 9 and 7(a)). Clarification of this discrepancy as well as of the asymmetry of the measured static coefficient for ϕ=7º and -7º is expected from additional testing to be carried out in the near future. The issue is particularly important since, as is shown below, the free-to-roll tests revealed that under some conditions the model did trim at ϕ=0.

Free-to-roll experiments were conducted using a variety of initial roll angles, however the initial roll rate was always zero due to characteristics of the experimental set-up. In all cases the model behaved in a stable fashion, surprisingly however, trim angles of 0 and ±21º were observed depending on the initial roll angle.

If the model was released from $40^o < |\phi| < \sim 60^o$ the trim angle was 21º on the same side as the initial roll angle. No tests were conducted with smaller release angles, but it can be expected that they would lead to the same trim conditions. However, if the initial roll angle exceeded $\sim|60^o|$, the model trimmed at 0º! Early attempts to understand this dependence on the initial roll angle did not lead to conclusive results; rather, as will be seen below, the process appears to depend on angular rates.

Simulations of the free-to-roll histories were conducted using the single degree-of-freedom equation of motion:

$$I\left(\frac{2V}{b}\right)^2 \ddot{\phi} + \left[c_1 + c_2\left(\frac{2V}{b}|\dot{\phi}|\right)^{c_3}\right]\mathrm{sgn}(\dot{\phi}) = C_l qSb$$

where the second term is a general model for the system friction. The values of the c's were determined by matching simulations with free-to-roll histories obtained under a variety of conditions. Attempts to ascribe viscous friction characteristics to the system (c_1=0, $c_2 \neq 0$ and c_3=1 as done e.g. by Elzebda et al.[10] did not result in reasonable simulations over the range of different conditions under consideration. Instead, it was found that only the c_1 term is required, i.e. the system has an approximately constant friction regardless of the angular velocity and load, which is consistent with sample tests conducted in order to determine the friction independently. The same value for c_1 was used in all simulations. Both locally linearized as well as fully non-linear simulations utilizing reaction surfaces were conducted.

Free-to-roll motion histories with an initial roll angle of approximately 40º, together with the corresponding non-linear and locally linear simulations are shown in Fig. 10 and 11. The locally linearized simulation was obtained using the static data depicted in Fig. 9 and the damping derivatives measured with $\Delta\phi$=5º for different values of ϕ_0 (Fig. 12). The non-linear simulation was conducted with the method described in Ref. 11, using the reaction surface for ϕ_0=14º, which contains the complete range of ϕ and $\dot{\phi}$ required by the simulation. Although both simulations trim at the correct roll angle, the locally linearized ones exhibit insufficient damping as well as a time delay, whereas the non-linear ones are generally in good agreement with the motion histories. An explanation for the damping insufficiency is found in Fig. 12, which shows that there is a significant dependence of the damping derivative on oscillation amplitude. This results in an underestimate of the damping when the free-to-roll motion amplitude is larger that the 5º used to obtain the derivatives. It should be noted that typically even smaller amplitudes would be used to obtain the derivatives, likely leading to more serious errors. The time delay is caused by the drop in restoring rolling moment for values of ϕ below 7º (Fig. 9), which causes the model to remain in that region for a longer period. This effect is more noticeable in Fig. 10 as in that case the roll angle more closely approaches zero due to the slightly higher release angle. It should be noted that the periods of subsequent cycles are in good agreement with those for the actual motions.

A free-to-roll test in which the model was released from a roll angle of 65.6º is depicted in Fig. 13, which also includes the corresponding locally linear and non-linear simulations. Since the locally linear simulation requires data for higher values of ϕ than in the previous cases, the additional static information was obtained from the

dynamic data were linearly extrapolated in Fig. 12. The locally linear simulation trims at -21º since, as mentioned before, it does not recognize the existence of an attractor of 0º. In this case the damping again proves to be insufficient and for the same reason as before. The frequency during the part of the simulation that involves zero crossings is too low due to the effect of the negative stiffness for $-7º < \phi < 7º$. Also note that the frequency in the latter part of the simulation, although higher, is still low compared to that of the actual motion.

In the case under consideration, the non-linear simulation was somewhat more involved as no individual reaction surface covered the full range of ϕ and $\dot{\phi}$. Therefore the simulation was started on the reaction surface corresponding to $\phi_0 = 42º$, which covers sufficiently high values of these quantities in the area of interest. As the simulation progresses, the trajectory on the phase plane leaves the domain covered by the original surface, requiring a small extrapolation until $\dot{\phi}$ reaches –0.1 which corresponds to the intersection between the zero and finite ϕ_0 reaction surfaces. Fig. 7 does not show the intersection because the angular rates used in the force tests were not quite high enough to reach it, although the trends of the various curves indicate that it exists. It was assumed that when the intersection was reached, the simulation should proceed on the $\phi_0 = 0$ reaction surface, as it was known *a priori* that it would result in the correct trim angle. Interestingly, the results proved to be very good in all respects, as can be observed in Fig. 13, where the first six symbols correspond to the simulation on the $\phi_0 = 42º$ surface and the rest on the 0º one. It should be noted that, although the actual model motion stops virtually exactly on the -21º attractor at the first overshoot peak, it does not remain there, indicating that the rolling moment is not zero, as would be the case if the reaction surfaces for $\phi_0 \neq 0$ and static data applied at that point of the simulation. Thus, the switch to the other flow regime must have occurred before that point, which is consistent with the procedure described above. Moreover, the higher frequency of the non-linear simulation is in better agreement with the actual motion than that in the latter part of the locally linearized one, again suggesting that the "stiffer" $\phi_0 = 0$ reaction surface (Fig. 9) better represents the flow conditions prevailing in that portion of the motion.

The possibility that the good agreement between the motion history and non-linear simulation is fortuitous cannot be ruled out at this stage. However, it seems more likely that it reflects the existence of an as yet unknown physical explanation for the assumed switch from the flow conditions represented by the $\phi_0 \neq 0$ reaction surfaces to the $\phi_0 = 0$ one, once their intersection is reached. Since the intersection is essentially determined by the angular rate (no ϕ effects in Fig. 7), this parameter very likely plays an important roll in the process. It bears mention that the angular rate for the cases shown in Figs. 10 and 11 never approached the intersection of the surfaces and thus no switching took place, even though at the first overshoot peak the actual motion stopped much closer to the attractor at 0º than the one at 21º. Flow visualization and unsteady surface pressure results are currently being used to supplement the data presented here in order to provide to fluid mechanics interpretation of the above phenomena. A discussion on the subject has been submitted for presentation[12].

10 Conclusions

Wind-tunnel rolling tests recently conducted on a 65º delta wing at 30º incidence have revealed the presence of severe aerodynamic non-linearities that are not amenable to treatment by a locally linearized mathematical model. Of particular interest is the existence of multiple roll attractors (trim angles) that seem to depend on the angular rate achieved during the motion.

Both non-linearities as well as attractor multiplicity could be handled well by simulations utilizing the hypersurface representation of air loads, suggesting that this approach can provide considerable improvements for the prediction of aircraft behaviour in the non-linear regime. Work is under way to elucidate the underlying physical causes of the observed phenomena.

11 Acknowledgements

We wish to acknowledge the support of the various individuals that, through their eager participation, made this work possible. We are particularly grateful to NAE's Low Speed Aerodynamics Lab. for providing the wind-tunnel time and personnel.

12 References

1. M.E. Beyers "Free-flight Investigation of High-maneuverability Missile Dynamics" AIAA J. of Spacecraft and Rockets Vol. 14, April, 1977.

2. M. Tobak, L. Schiff "Aerodynamic Mathematical Modeling - Basic Concepts" AGARD Lecture Series LS-114, 1981.

3. K.J. Orlik-Rukemann "Aerodynamic Aspects of Aircraft Dynamics at High Angles of Attack" Presented at AIAA AFM Conf. Aug., San Diego, CA 1982, AIAA-82-1363. Also in AIAA J. of Aircraft Vol. 20, Sept., 1983.

4. J. Kalviste "Use of Rotary Balance and Forced Oscillation Test Data in a Six Degrees of Freedom Simulation" Presented at AIAA AFM Conf. Aug., San Diego, CA, 1982, AIAA-82-1364.

5. E.S. Hanff "Dynamic Non-linear Airloads-Representation and Measurement" Presented AGARD Symposium on Unsteady Aerodynamics - Fundamentals and Applications to Aircraft Dynamics, Göttingen, Germany, May, 1985, AGARD CP-386.

6. E.S. Hanff "Determination of Non-linear Loads on Oscillating Models in Wind Tunnels" Presented at IEEE Int. Con. On Instrumentation in Aerospace Simulation Facilities, St. Louis, France, Sept., 1983, ICIASF'83 Record.

7. E.S. Hanff, K. Kapoor, C.R. Anstey "Large-amplitude High-rate Roll Oscillation System for the Measurement of Non-linear Loads" Submitted for presentation at the AIAA16th Aerodynamic Ground Testing Conf. June, 1990.

8. E.S. Hanff, S.B. Jenkins, A. Prini "Instrumentation and Other Issues in Non-linear Dynamic Testing in Wind Tunnels, Presented at IEEE Int. Con. On Instrumentation in Aerospace Simulation Facilities, Stanford University, Aug., 1985, ICIASF' 85.

9. A.S. Arena, R.C. Nelson "The Effect of Asymmetric Vortex Wake Characteristics on a Slender Delta Wing Undergoing Wing Rock" Presented at AIAA AFM Conf. Aug., Boston, 1989, AIAA-89-3348.

10. J.M. Elzebda, A.H. Nayfeh, D.T. Mook "Development of an Analytical Model of Wing Rock for Slender Delta Wings" AIAA J. of Aircraft Vol.26, Aug., 1989.

11. E.S. Hanff, S.B. Jenkins "A Method for Non-linear Flight Mechanics Simulations" Presented at IEEE Int. Con. On Instrumentation in Aerospace Simulation Facilities, Göttingen, Germany, Sept., 1989.

12. E.S. Hanff, L.E. Ericsson "Multiple Roll Attractors of a Delta Wing at high Incidence" Submitted for presentation at the AGARD Symposium on Vortex Flow Aerodynamics, Scheveningen, Holland, Oct., 1990.

13 Figures

N.B.: These figures were scanned from a copy of the published paper after the original artwork was lost. The authors would like to apologize for the poor quality.

An additional laser-sheet flow visualization photograph has been included on page 13.

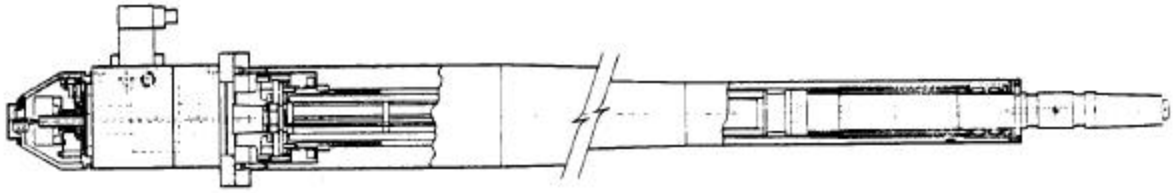

Fig.1 Large-amplitude high-rate roll rig

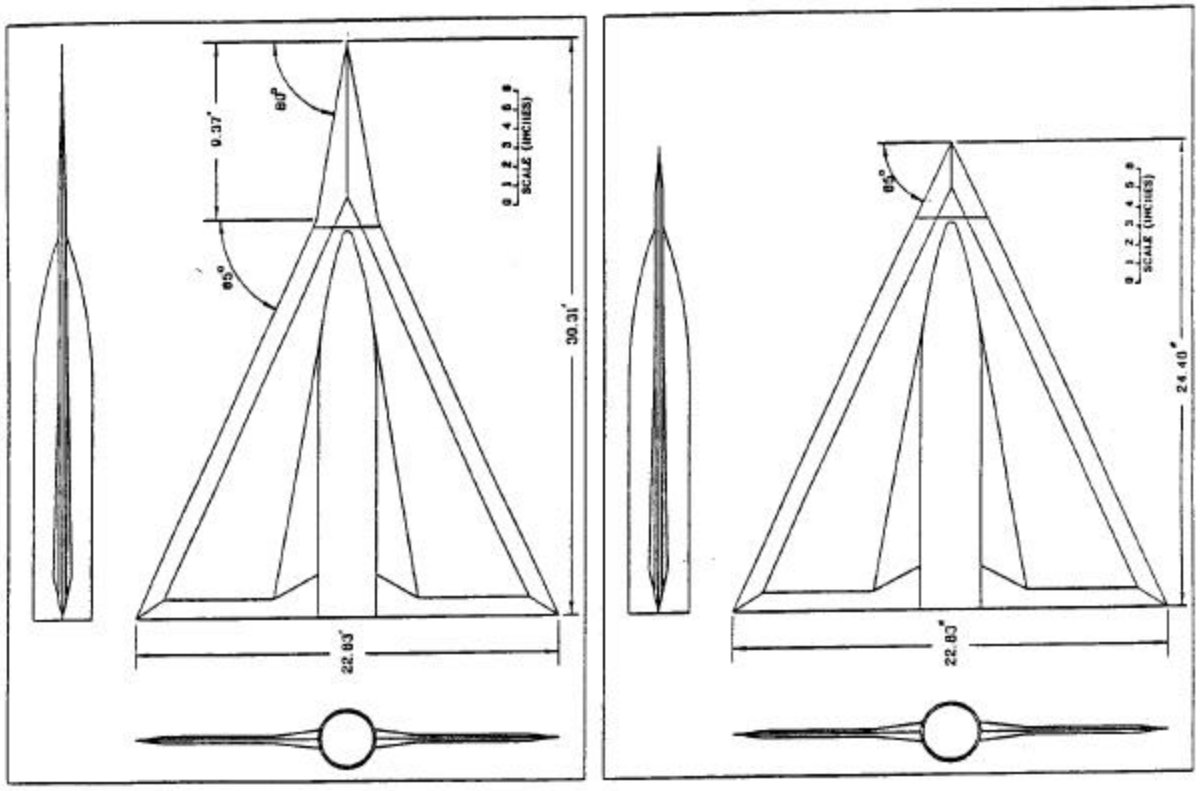

Fig.2 Delta wing composite model

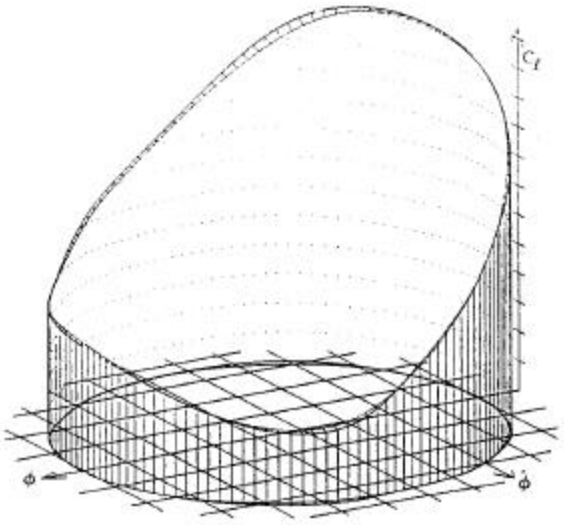

Fig.3 Repeat run with two different balances

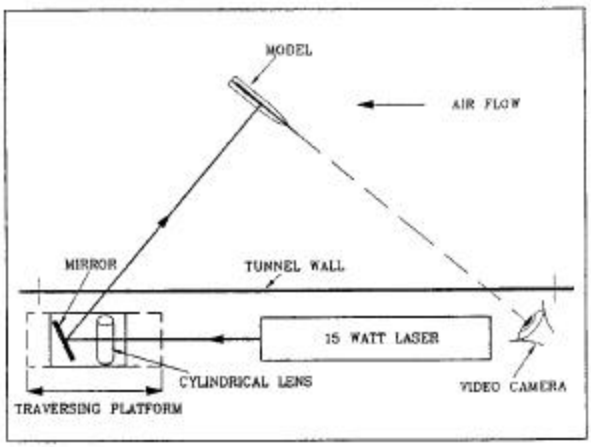

Fig.4 Laser-sheet flow visualization arrangement

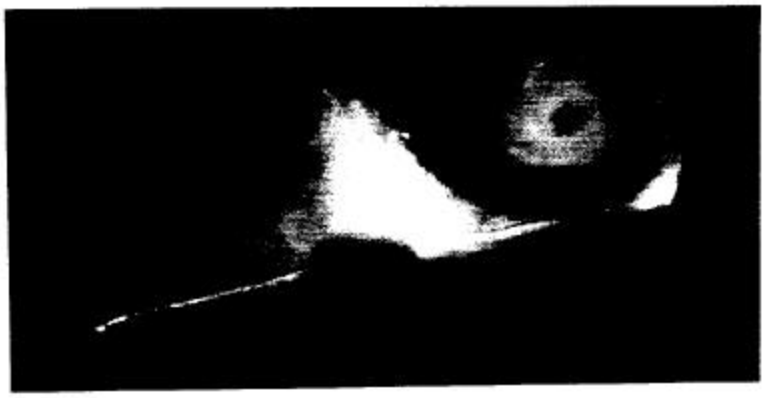

Fig.5 Laser-sheet flow visualization of 65° delta

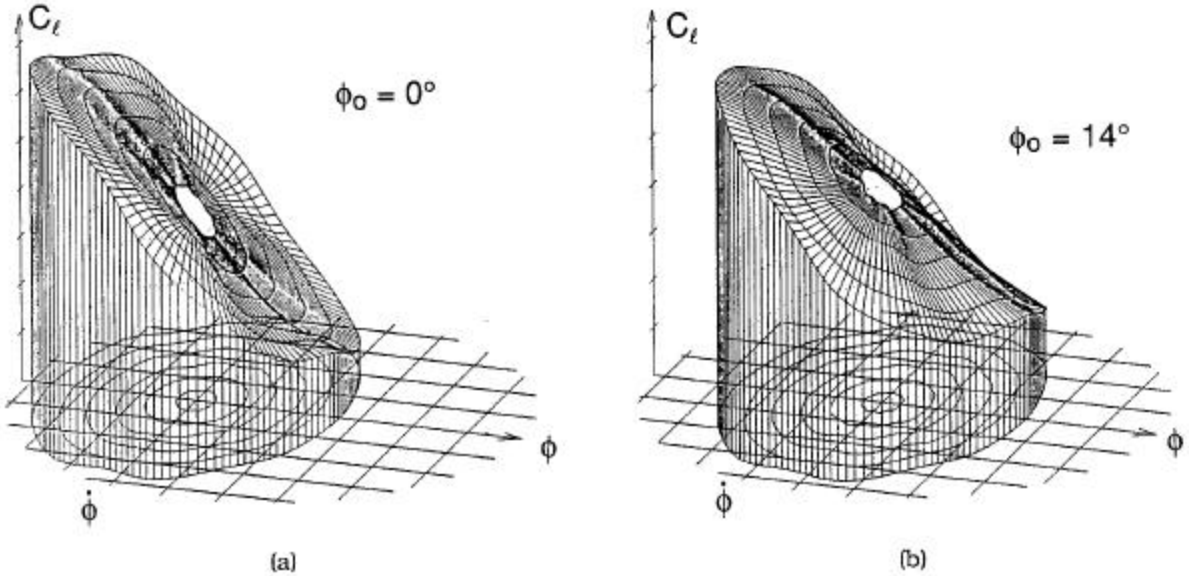

Fig.6 Reaction surfaces for α=30° at k=0.14

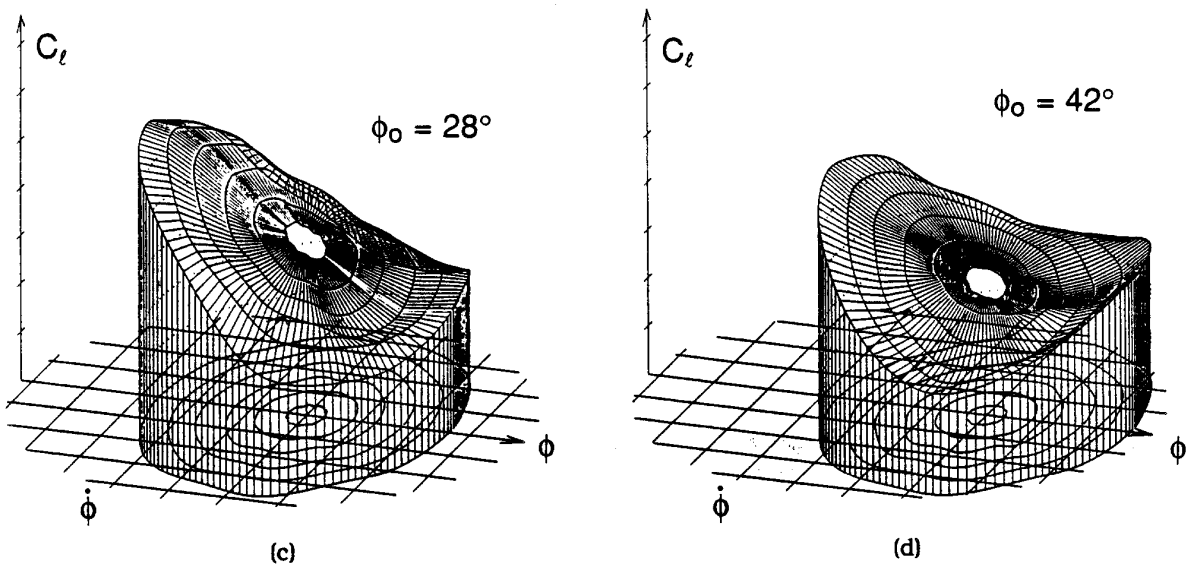

Fig. 6 Reaction surfaces for α=30° at k=0.14 (Continued)

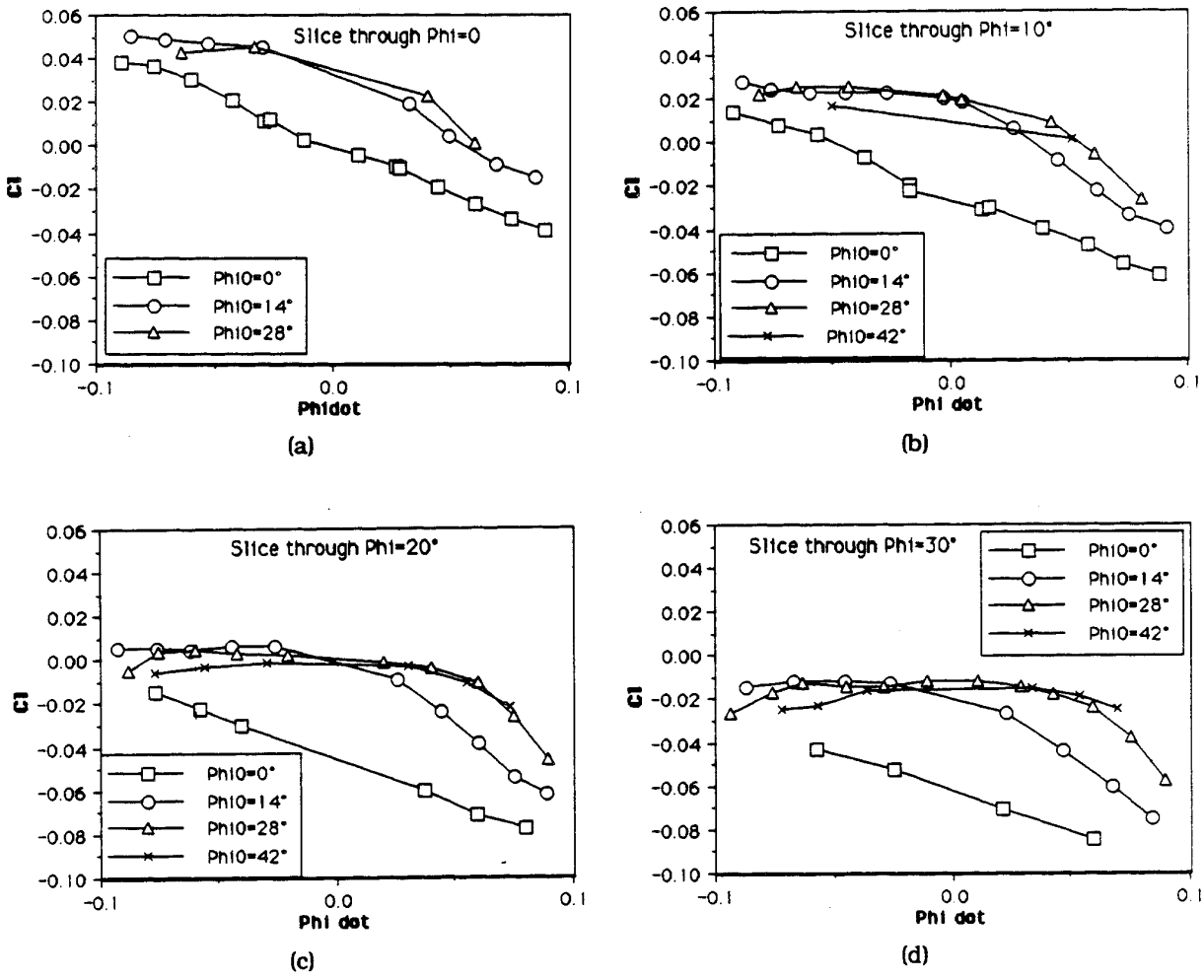

Fig.7 Intersection of reaction surfaces with fixed ϕ planes

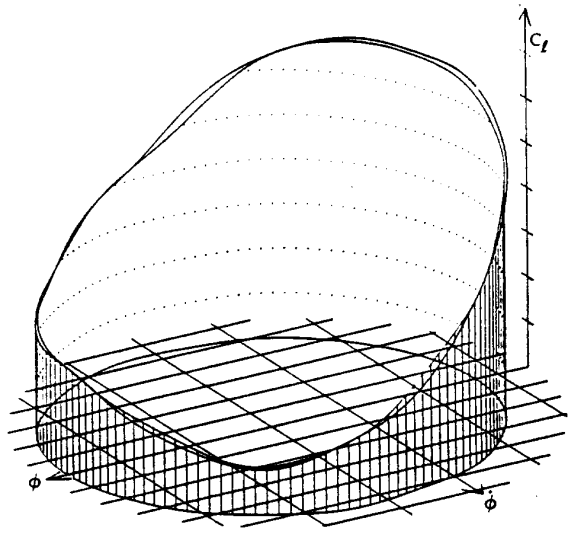

Fig.8 Load point trajectories for ϕ_0 =14° and -14°

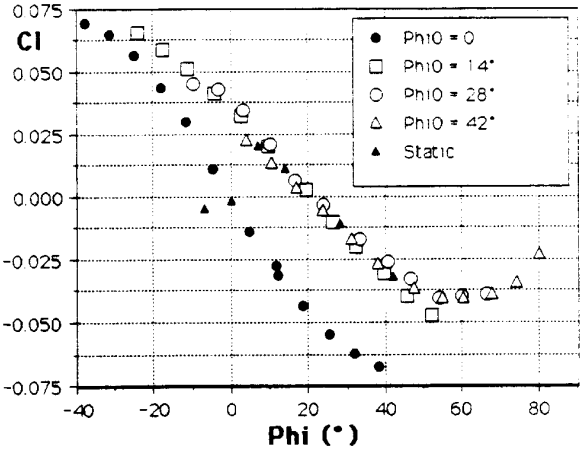

Fig.9 Intersection of surfaces with $\dot{\phi}$=0 plane

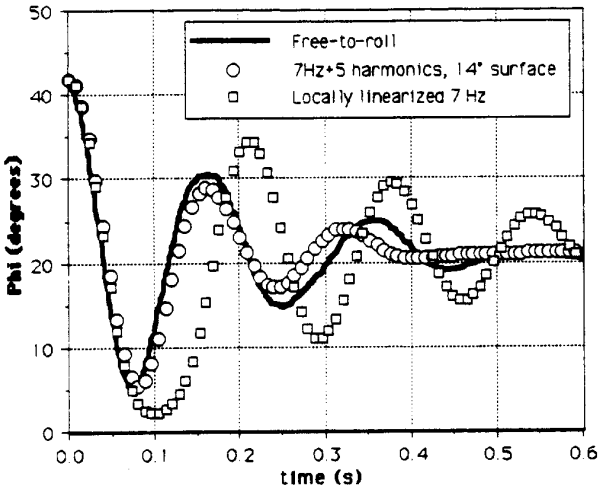

Fig.10 Motion history and simulations:ϕ(0)=41.4°

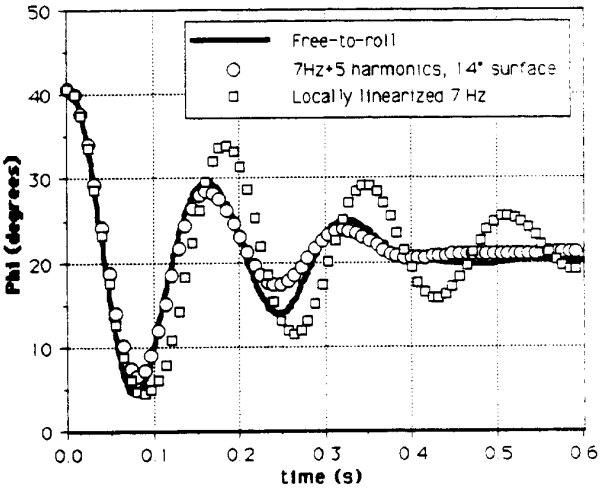

Fig.11 Motion history and simulations:ϕ(0)=40.5°

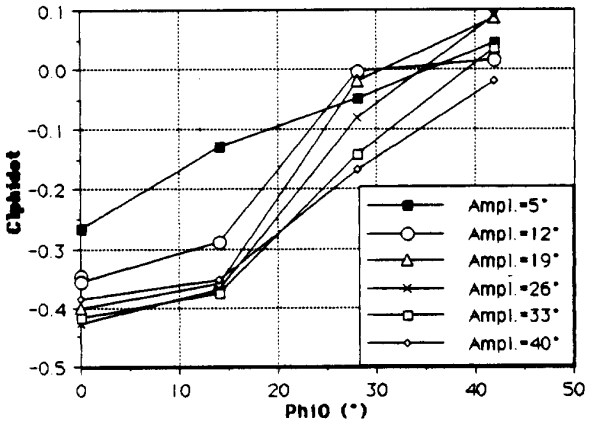

Fig.12 Effect of amplitude on damping derivative

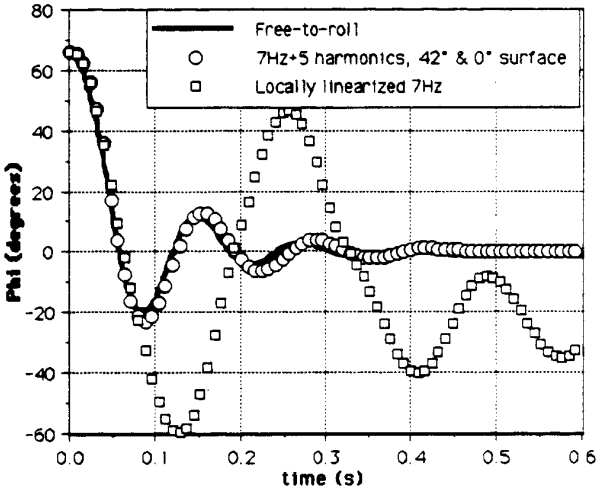

Fig.13 Motion history and simulations:ϕ(0)=65.6°